Oil Shale, 2023, Vol. 40, No. 3, pp. 194–211
doi: https://doi.org/10.3176/oil.2023.3.02
ISSN 0208-189X

Experimental study on the thermophysical properties of Jimsar oil shale

Zhijun Liu[(a,b)*], Haotian Ma[(a)], Zhen Wang[(a)], Yuzhen Guo[(a)], Wei Li[(a)], Zhiyuan Hou[(a,b)]

[(a)] College of Mining Engineering, Heilongjiang University of Science and Technology, Harbin 150022, China
[(b)] Heilongjiang Ground Pressure and Gas Control in Deep Mining Key Laboratory, Heilongjiang University of Science and Technology, Harbin 150022, China

Received 28 January 2023, accepted 14 July 2023, available online 10 September 2023

Abstract. *Oil shale is a potential strategic reserve resource and a significant supplementary energy source due to its huge reserves and numerous utilization methods. The study of oil shale thermophysical properties can provide significant guidance for proposed in-situ mining. Taking the oil shale in Jimsar, Xinjiang as an example and using thermophysical experiments, this paper studies the variation in thermophysical properties of oil shale with temperature. The results show that the specific heat capacity of oil shale increases with increasing temperature below 390 °C, but the change decreases with increase of temperature; however, when the temperature exceeds 390 °C, the specific heat value change fluctuates irregularly. At 31–720 °C, the thermal expansion of oil shale indicates obvious anisotropy. Namely, in the vertical bedding direction, the thermal expansion rate manifests a typical two-stage increase, while in the parallel bedding direction, the thermal expansion coefficient exhibits an overall increasing trend but fluctuates significantly due to the reaction of components within the oil shale.*

Keywords: *thermophysical properties, Jimsar oil shale, specific heat capacity, thermal expansion, anisotropy.*

1. Introduction

2022 is a year of intertwined crises, which reinforces the need for balance in the dimensions of energy security, affordability, and sustainability. The need to balance energy security, equity (affordability) and environmental sustainability has never been more pressing, and the diversity of challenges

* Corresponding author: e-mail *2004800167@usth.edu.cn*

faced by countries is clearer than ever [1]. As energy resource depletion is impending, oil shale has become an important strategic energy source due to its large reserves, great potential and numerous methods of utilization [2]. China's oil shale reserves are approximately 330 billion barrels, ranking second in the world. Therefore, there is a great potential for the exploitation and utilization of this energy in China [3].

The methods of oil shale conversion can be divided into dry distillation and underground in-situ mining. However, considering the advantages of large recoverable depth, high oil recovery rate, land occupation, and environmental protection, the in-situ mining has become a new trend in the development of oil shale mining technology. Regardless of the mining method, the output of shale oil and gas is always related to the pyrolysis of the solid kerogen [4–6]. In-situ mining refers to the process of pyrolysis of the solid kerogen into liquid or gaseous hydrocarbon at high temperatures underground by means of electricity [7, 8], fluid [9], or gas [10]. Due to the pyrolysis of kerogen and the thermal reaction of inorganic minerals, the thermophysical properties of oil shale, such as thermal conductivity, specific heat capacity and thermal expansion coefficient, are bound to change accordingly, which directly affects the rock's pyrolysis efficiency and, consequently, the output of shale oil and gas.

In the in-situ mining by superheated steam, the thermal expansion of oil shale has a great influence on its stability during this process, while the variation in specific heat capacity directly determines the oil shale heating capacity. This has attracted a lot of scholars to undertake research in the respective field. Compared with other rocks such as sandstone and granite, oil shale contains a unique organic matter, kerogen. With increasing temperature, oil shale will be pyrolyzed to generate shale oil and gas. The pyrolysis process can be divided into three stages [11–15] and is also affected by many factors, such as the heating rate [16–18], the size of oil shale particle [19] and the degree of oil shale metamorphism [20, 21]. Many investigators have studied the variation in the thermophysical properties of rocks with temperature. It is found that the thermal conductivity and thermal diffusivity of rocks are mostly anisotropic [22–24] and the variation in their anisotropy coefficients is also different. Even though the specific heat capacity of most rocks is positively correlated with temperature, thermal conductivity and thermal diffusion coefficient are often negatively correlated with temperature [24–28]. It is also found that minerals, pores, temperature, and pressure are the factors determining the specific heat capacity [29–31]. However, due to the characteristics of high-temperature pyrolysis of oil shale, the current studies on its thermophysical properties are generally conducted in the low-temperature region (31–390 °C), or the specimens are heated to the target temperature and kept for a certain period of time and then their thermophysical properties are measured after they have been moved and cooled down to room temperature. It was found that the specific heat capacity of oil shale increased first and then

decreased with increasing temperature, and the thermal conductivity shows an overall decreasing trend [24, 32, 33]. In the in-situ mining, the thermal expansion of oil shale has a great influence on the rock stability [34]. In this regard, many scholars have found that due to the thermal expansion properties under thermal action, new pores could be produced in the rock to strengthen its internal connectivity [35–38]. Also, some sensitive temperature ranges for thermal expansion of certain rocks could be determined [39, 40], while significant differences in this parameter exist among the rocks parallel and vertical to the bedding [41–44]. Because of the pyrolysis characteristics of oil shale at high temperature, the variation in the thermal expansion at this stage is highlighted in real-world engineering applications.

In summary, the majority of previous studies focus on the thermophysical properties of shale and sandstones or on those of oil shale in the low-temperature stage. At the same time, studies regarding the thermophysical properties of the latter in the high-temperature pyrolysis stage are scarce in the literature. In the in-situ mining, the thermophysical properties of oil shale at high temperature are crucial to its stability and the exploitation of oil and gas, while the specific heat capacity and thermal expansion of the rock directly affect the evolution of oil shale pore space. Therefore, the purpose of this study is to research the real-time variation in the specific heat capacity and thermal expansion of Jimsar oil shale with temperature, and provide the theoretical basis for the oil shale in-situ mining.

2. Materials and methods

2.1. Preparation of oil shale samples

Oil shale samples were collected from the Shichanggou Mine of Jimsar County, Xinjiang, China, and sealed immediately using paraffin wax to avoid weathering and deterioration. Raw oil shale samples were gathered, crushed and cut along parallel and vertical bedding directions into the size of 3 mm × 3 mm × 25 mm, and then subjected to thermal expansion experiments. Later, some of the samples were ground and sieved to a grain size below 75 μm [45], according to the National Standards of China (DZ/T 0276), and then dried for 8 h at 70 °C in an oven, and finally stored in a desiccator for the specific heat capacity experiments.

According to Liu et al. [14], the primary mineral components of Jimsar oil shale are quartz, plagioclase and dolomite, followed by sanidine, calcite, clay minerals and smaller amounts of pyrite and gypsum. The results of the thermogravimetric (TG) experiment showed that the total weight loss of oil shale was 20.4% in the temperature range of 31–800 °C, and the pyrolysis was a typical three-stage process. The first stage was conducted at 31–390 °C, with a weight loss of about 1.3%. The second stage was carried out at 390–540 °C.

This stage was further divided into two substages, I and II. The weight loss at stage I (399–488 °C) was about 12.2%, and at stage II (488–540 °C) 2.3%. The third stage was performed at 540–800 °C, with a weight loss of 4.6%. The results show that the TG curve is closely related to the organic and inorganic mineral composition of oil shale [11].

2.2. Experimental process

The specific heat capacity of oil shale was measured in the laboratory, using a differential scanning calorimeter (DSC200F3) (Fig. 1). The thermal expansion experiment was conducted using a thermal dilatometer (DIL402PC) (Fig. 2).

In the specific heat capacity experiment, approximately 20 mg of oil shale powder was evenly distributed at the bottom of the thermogravimetry crucible, and then heated to 720 °C at a rate of 0.5 °C/min using Ar gas as a protective gas at a flow rate of 100 ml/min. Later, the variation in the specific heat capacity from 31–720 °C was obtained with Origin 2021 software.

In the thermal expansion experiment, the DIL402PC resolution was 8 nm. The specimens with parallel and vertical beddings were placed in the heating furnace in turn for the experiment. Under the protection of Ar gas, the specimens were heated from room temperature to 720 °C at a heating rate of 3 °C/min. Then the variation in the thermal expansion coefficient and thermal expansion rate at 31–720 °C can be obtained by the Origin 2021 software.

Fig. 1. DSC200F3 differential scanning calorimeter.

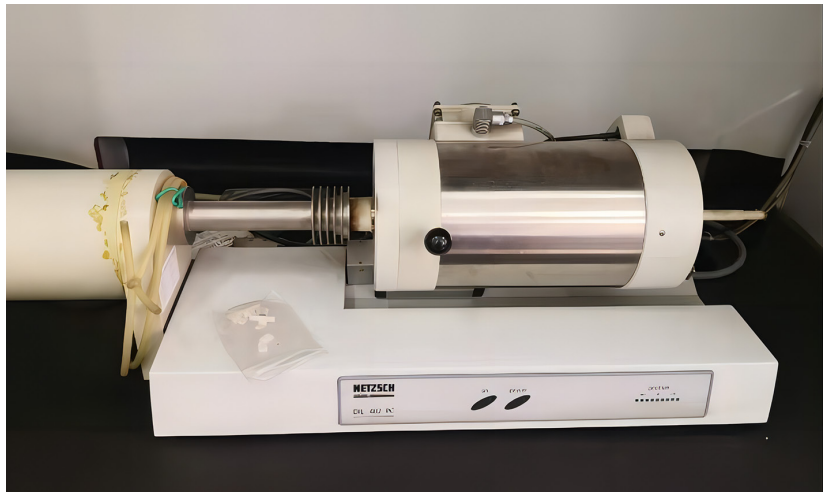

Fig. 2. DIL 402 PC thermal dilatometer.

3. Results and discussion

3.1. The variation in specific heat capacity with temperature

The specific heat capacity (C) is the heat absorbed (or released) by a unit mass of rock when the temperature rises (or drops) by 1 °C. Figure 3 shows the variation in the specific heat capacity of oil shale as the temperature increases, during which the actual test temperature is 31–600 °C because oil shale pyrolysis products will pollute the detector probe when it exceeds 600 °C.

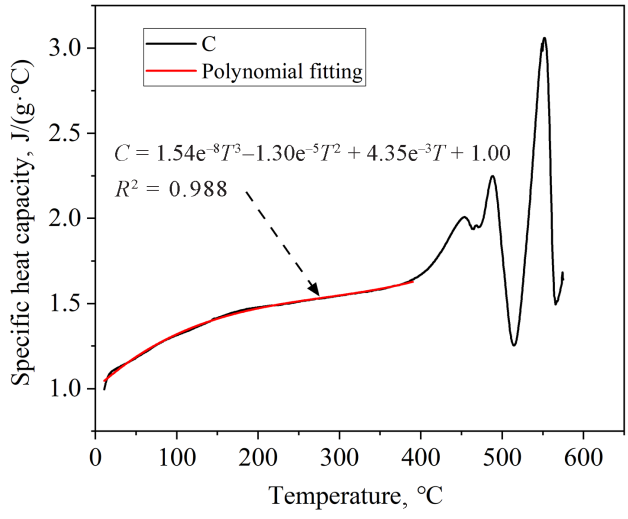

Fig. 3. Oil shale specific heat capacity versus temperature.

As shown in Figure 3, the specific heat capacity of oil shale increases with temperature before 390 °C, but the value variation scales down; however, when the temperature exceeds 390 °C, the specific heat capacity fluctuates irregularly. In the temperature range of 31–390 °C, the specific heat capacity of oil shale increases with ascending temperature. At 31 °C, the specific heat capacity is 1.11 J/(g·°C). The value increases by 47.7% at 390 °C, reaching 1.64 J/(g·°C). During this process, the moisture inside oil shale has a little effect on its specific heat capacity, mainly because the sample has been dried at 75 °C for 3 hours before the test [46, 47]. The reason for the increase of the specific heat capacity with the temperature rising from 31 °C to 200 °C is that the water with a high specific heat evaporates from the gypsum and fills the pores [46, 48]. As the temperature increases, the evaporation of mineral crystalline water from oil shale causes a steady decrease in the slope of the specific heat capacity curve.

However, in the temperature range of 200–390 °C, the slope of the curve is roughly constant, and the growth of the specific heat capacity tends to be more regular. By fitting the curve of this temperature range, the corresponding function is obtained and shown in Formula (1):

$$\begin{cases} C = 1.00 + 4.35 \times 10^{-3} T - 1.30 \times 10^{-5} T^2 + 1.54 \times 10^{-8} T^3 \\ R = 0.998 \end{cases}, \qquad (1)$$

where C is the specific heat capacity, J/(g·°C), and T is the temperature, °C.

After the temperature exceeds 390 °C, the specific heat capacity of oil shale indicates erratic variations, which suggests that some reactions inevitably take place inside the rock. As the temperature grows from 390 °C to 540 °C, the specific heat capacity of oil shale first surges to a characteristic peak value of 2.01 J/(g·°C) at 453.5 °C. It is mainly attributed to the fact that substantial energy is required for the pyrolysis of kerogen within oil shale to generate gas, and aliphatic and aromatic compounds in stage I [49]. The comprehensive pyrolysis of kerogen leads to a decline in the specific heat capacity of oil shale. However, the release of the generated gas creates new pores in oil shale [50–52] while the aliphatic and aromatic compounds fill some of these pores in preparation for secondary reactions in stage II, bringing about an increase of the specific heat capacity of oil shale [11]. Moreover, as the temperature rises, the specific heat capacity of inorganic minerals contained in oil shale also increases [11]. Thus, with the interaction of these reactions, the specific heat capacity exhibits an overall ascending trend in stage I and reaches a peak value of 2.25 J/(g·°C) at 488.5 °C. From 490 °C to 527 °C, the specific heat capacity of oil shale decreases significantly, reaching a minimum value of 1.25 J/(g·°C) at 514.5 °C. It is mainly ascribed to the secondary reaction of aliphatic and aromatic compounds in stage II, during which these compounds crack and generate a large amount of gas. Consequently, the original pores recover and oil shale expands to a certain extent, forming some new pores.

In the temperature range of 540–600 °C, the specific heat capacity curve of oil shale first rises, then dips and thereafter climbs again to the peak of 3.06 J/(g·°C) at 552 °C, but afterwards, a trough of 1.49 J/(g·°C) emerges at 565.5 °C. Combined with the mineral fraction of oil shale, the pyrite in it needs to absorb a large amount of heat before decomposition, resulting in a bulge in the specific heat capacity of the rock. However, after the temperature reaches 552 °C, the specific heat capacity of oil shale decreases rapidly, but still remains higher than 1.25 J/(g·°C). It is because other inorganic minerals in oil shale are relatively stable before 565.5 °C, and its specific heat capacity still increases with increasing temperature [11]. After the temperature reaches 565.5 °C, the specific heat capacity of oil shale continues to increase. The reason is that the α and β phase transformation of quartz at 574 °C necessitates a tremendous accumulation of energy and the heat energy absorbed is turned into activation energy for the reactions [53].

In summary, the variation in the specific heat capacity of oil shale is closely related to its material composition. At 31–390 °C, the components of oil shale are stable and its specific heat capacity increases in a certain pattern with rising temperature. However, at 390–600 °C, the specific heat capacity curve shows irregular fluctuations under the combined effect of kerogen pyrolysis, pyrite thermal decomposition and other factors. This indicates that the material composition of oil shale determines its thermophysical properties.

3.2. The variation in thermal expansion with temperature

In general, the thermal expansion of oil shale is greatly influenced by its components. With the increase of temperature, the components of oil shale undergo a series of physical and chemical changes, which directly affect its thermal expansion and evolution of internal pore space. Figure 4 illustrates the variations in the thermal expansion rate and coefficient of oil shale with temperature in parallel and vertical bedding directions.

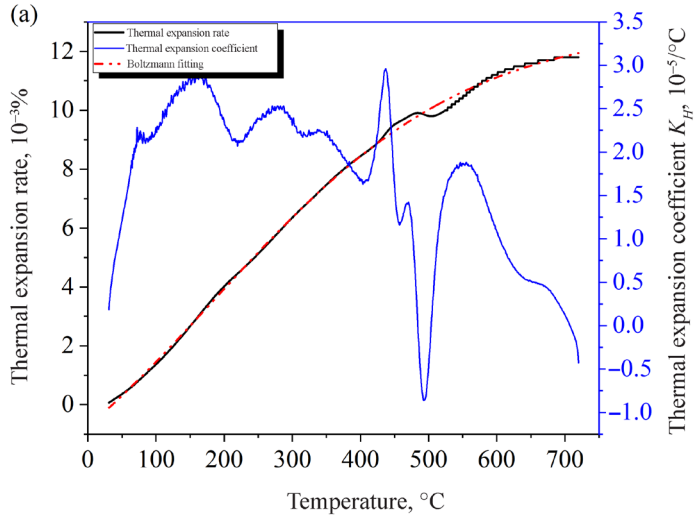

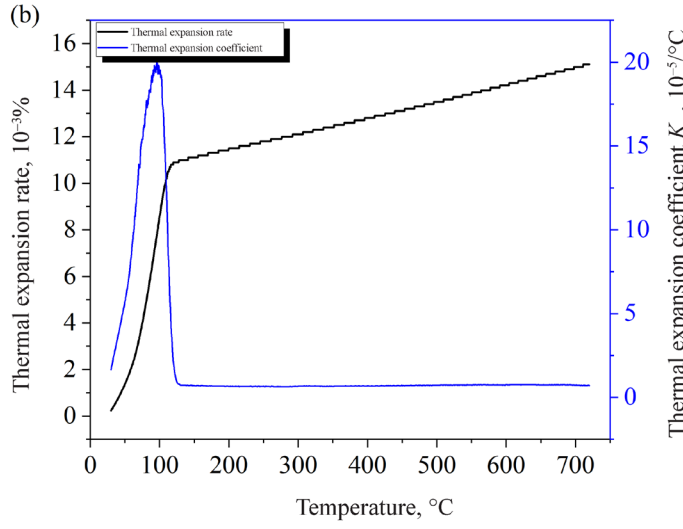

Fig. 4. Curves of oil shale thermal expansion versus temperature in (a) parallel bedding direction and (b) perpendicular bedding direction.

Figure 4a shows the variation in the thermal expansion coefficient and rate of oil shale with temperature in the parallel bedding direction. At 31 °C, the oil shale thermal expansion coefficient (K_H) is 0.186 × 10^{-5}/°C. K_H then increases as the specimen is heated to 180 °C, peaking at 164.5 °C with a value of 2.9 × 10^{-5}/°C. Subsequently, in the temperature range of 180–390 °C, K_H shows a descending trend and fluctuations, with one peak of 2.52 × 10^{-5}/°C appearing at 282 °C and another peak of 2.25 × 10^{-5}/°C at 340 °C, the minimum value being 1.77 × 10^{-5}/°C at 390 °C. Between 390 °C and 540 °C, K_H first increases sharply and then undergoes a drastic decline, reaching a peak value of 2.96 × 10^{-5}/°C at 437 °C and a minimum value of –0.862 × 10^{-5}/°C at 493 °C. In the temperature range of 540–720 °C, K_H first increases and then decreases stepwise, peaking at 555 °C with a value of 1.88 × 10^{-5}/°C and smoothing out at around 660 °C with a value of 0.484 × 10^{-5}/°C. When the temperature is higher than 708 °C, K_H is less than 0. Therefore, it can be deduced that K_H basically remains greater than 0, indicating that between 31 °C and 720 °C, oil shale is mainly in a state of expansion in the parallel bedding direction.

According to Figure 4a as well as the variation in K_H, the thermal expansion rate of oil shale primarily shows an increasing trend in the parallel bedding direction. In the temperature range of 31–100 °C, the expansion rate curve is concave. Based on the above analysis of the specific heat capacity, the main reason is that the dehydration of gypsum in oil shale at the initial stage of heating lowers the internal temperature and the mineral particles have not yet fully expanded [11, 46]. As a result, the expansion rate of oil shale grows slowly, which is consistent with the variation in its specific heat capacity in this temperature range. With the evaporation of mineral crystalline water, the

internal temperature of oil shale gradually stabilizes. In the temperature range of 100–390 °C, the oil shale internal components are less constrained due to the presence of the original pores inside it, and keep expanding when the rock is heated, so the K_H value rises [44, 54]. However, as the thermal expansion intensifies, the constraint between the components strengthens, leading to a decrease in K_H, which agrees with the fluctuation of K_H in this temperature range. After the temperature exceeds 390 °C, the thermal expansion rate increases with temperature and reaches a peak value of 9.91×10^{-3}% at 484 °C. Combined with the specific heat capacity analysis, it is evident that when the gas generated in stage I is released, numerous new pores form, which weaken the mineral skeleton strength of oil shale. Meanwhile, the generated aliphatic and aromatic compounds block some pores [55, 56], and with rising temperature, the expansion force is enhanced, leading as a result to the fracture of the original bedding structure of oil shale and damage to its mineral skeleton [57]. From 484 °C to 540 °C, the aliphatic and aromatic compounds undergo secondary and pyrolysis reactions and are transformed into shale oil and gas to escape from the pores inside oil shale. At the same time, the pores expand and the pore connectivity is improved to promote oil and gas transport [51], while the mineral skeleton produces a certain degree of shrinkage, which is the difference in thermal expansion between oil shale and other rocks, during which the expansion rate of oil shale decreases and reaches a trough value of 9.8×10^{-3}% at 506 °C. Therefore, under the combined effect of these factors, the oil shale structure may fracture during the in-situ mining, blocking the transport of the heat transfer medium and terminating oil shale pyrolysis. In the temperature range of 527–720 °C, the thermal expansion rate of oil shale continues to grow, but the K_H value gradually decreases. It is mainly due to the decomposition of pyrite and illite within the weakening local parts of oil shale [54]. Meanwhile, as the main inorganic mineral within oil shale at this stage, quartz undergoes α and β phase transformation at 574 °C and expands in volume [53], thus strengthening the rock stability. However, when the temperature is higher than 600 °C, carbonate minerals such as dolomite in oil shale are decomposed [11, 12], and the partial collapse of the mineral skeleton further slows down its expansion rate. This explains K_H being less than 0 after the temperature reaches 708 °C [50].

Figure 4b illustrates the variations in the oil shale thermal expansion coefficient and thermal expansion rate with temperature in the vertical bedding direction. At 31 °C, the thermal expansion coefficient of oil shale (K_V) is 1.87×10^{-5}/°C. As the temperature is raised to 190 °C, K_V initially rises sharply and then decreases, reaching a peak value of 20.3×10^{-5}/°C at 96.5 °C. Afterwards, K_V plunges to 0.662×10^{-5}/°C at 190 °C. In the temperature range of 190–720 °C, K_V maintains a value of 0.707×10^{-5}/°C.

Within 31–720 °C, the oil shale thermal expansion rate in the vertical bedding direction exhibits a typical two-stage growth trend (Fig. 4b). Specifically, this rate increases sharply at temperatures between 31 °C and

115 °C, while the increase rate slows down after the temperature exceeds 115 °C. When the temperature of oil shale is between 31 °C and 115 °C, the mineral crystalline water generated inside it boils and expands, creating interlayer fractures that dramatically accelerate the oil shale expansion in the vertical bedding direction [58], and facilitating subsequent oil and gas transportation. In the temperature range of 115–720 °C, the components of oil shale expand thermally. When the expansion direction crosses the bedding vertically, oil shale is pulled, while pore fissures, gas, and water get non-uniformly distributed in the bedding. Additionally, microstructural planes, which are obliquely intersected with the bedding direction, and secondary structure surfaces are generated with elevating temperature. The formation of these structures provides the space for oil shale expansion. The expansion rate of oil shale deaccelerates, promoting the formation of more interlaminar fissures, thereby boosting the transportation of oil and gas in it. Hence, the thermal expansion rate of oil shale shows continuous slow growth [50].

Based on the above analysis, it is evident that temperature has a considerable impact on the anisotropy of the thermal expansion coefficient of oil shale, which is expressed as anisotropy coefficient (K_H/K_V). The variation in the K_H/K_V value with increasing temperature is depicted in Figure 5. The overall variation in K_H/K_V with temperature consists of 4 stages. In the first stage, in the temperature range of 31–119 °C, K_H/K_V preliminarily decreases slowly and then increases dramatically, and the minimum value of 0.1116 is achieved at 98.5 °C. In the second stage, when the specimen is heated from 119 °C to 390 °C, K_H/K_V initially increases rapidly from 1.1195 to 4.2213, but after the

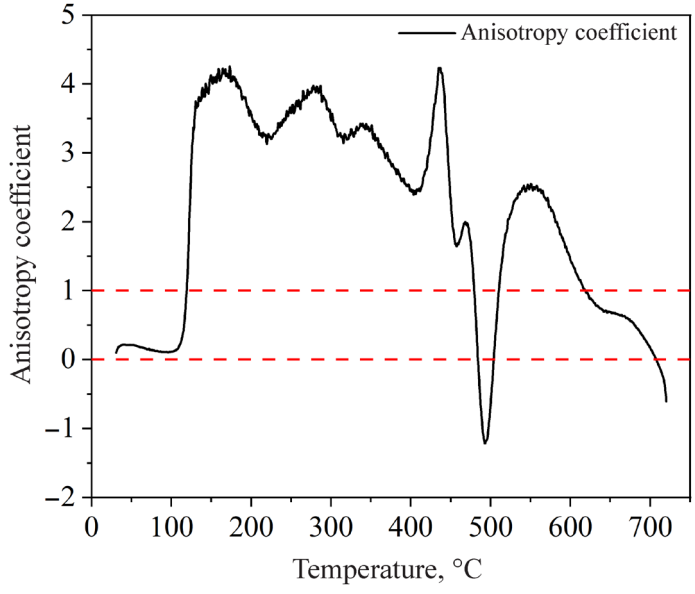

Fig. 5. Anisotropy coefficient versus temperature.

temperature reaches 164.5 °C, its value displays a downward trend. There are two abrupt changes in K_H/K_V in the temperature range of 164.5–390 °C, and two peak values of 3.9623 and 3.3534 are achieved at 282 °C and 345 °C, respectively. In the third stage, within 390–540 °C, K_H/K_V first increases to a peak value of 4.2363 at 435.5 °C, then decreases rapidly to –1.2141 at 493 °C, increasing finally again. In the fourth stage, as the temperature rises from 540 °C to 720 °C, K_H/K_V first increases from 2.1833 to 2.5546 at 550.5 °C and then decreases to –0.6068. Therefore, it can be concluded that in the temperature ranges of 119–484 °C and 510.5–618.5 °C, K_H is far larger than K_V. In the other two temperature ranges, K_V is higher than K_H.

The variation in K_H has poor regularity, which brings great inconvenience to the subsequent processing and practical application of material. By comparison, the fitting curve has better stability, for which the Boltzmann equation is adopted to fit the thermal expansion rate curve (Fig. 4a).

The temperature derivative curve fitting results are summarized in Figure 6a. Since the variation in K_V is regular, it is fitted directly; the results are shown in Figure 6b. The corresponding functions are represented by Formula (2) and Formula (3), respectively:

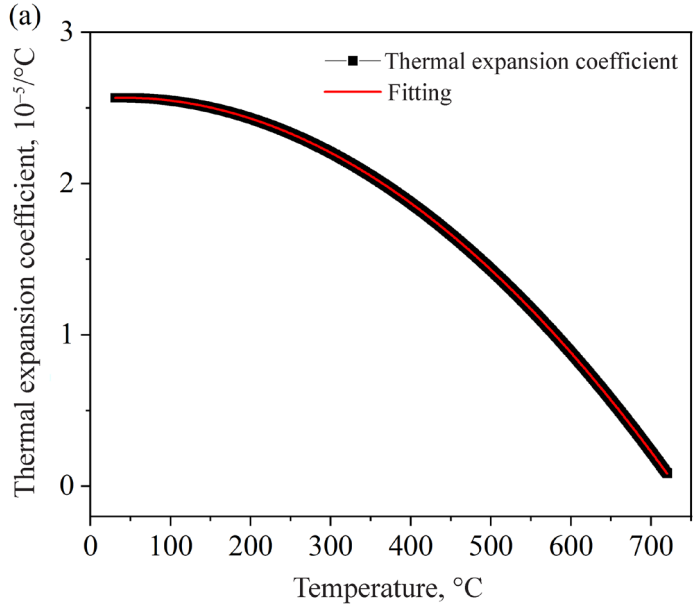

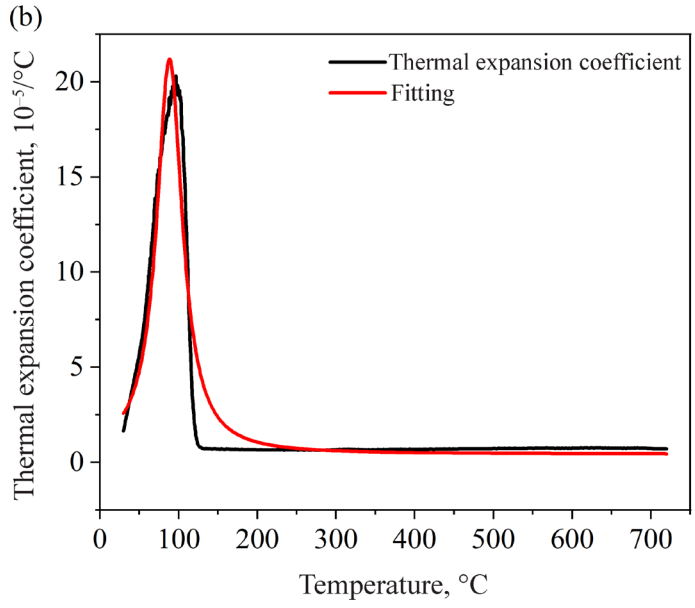

Fig. 6. Fitting curves of oil shale thermal expansion versus temperature in the (a) parallel bedding direction and (b) perpendicular bedding direction.

$$K_H = 2.559\times10^{-5} + 4.329\times10^{-9}T - 5.375\times10^{-11}T^2, \quad (2)$$

$$K_V = 4.43\times10^{-6} + 8.554\times10^{-3}\left(\frac{41.807}{4(T-87.796)^2 + 1747.839}\right), \quad (3)$$

where K_H is the thermal expansion coefficient in the direction of parallel bedding, 10^{-5}/°C, K_V is the thermal expansion coefficient in the direction of vertical bedding, 10^{-5}/°C, and T is the temperature, °C.

In summary, the specific heat capacity and thermal expansion of oil shale play a vital role in in-situ mining by superheated steam. The variation in the specific heat capacity directly determines the heating capacity of oil shale. The thermal expansion exhibits significant variability due to the anisotropy of oil shale, and the variation in thermal expansion in parallel and vertical bedding directions straightly affects the transfer of the heat transfer medium in oil shale and the transportation of oil shale products. Therefore, how to maintain the stability of oil shale during pyrolysis is an urgent issue to be dealt with in the process of its in-situ mining. In this section, the variations in the thermal expansion and the specific heat capacity of oil shale with temperature are analyzed, the results provide a scientific foundation for the design of in-situ oil shale mining.

4. Conclusions

In this paper, the results of experiments conducted to examine the variation in the thermophysical properties of Jimsar oil shale with temperature are presented. Meanwhile, the anisotropy of the thermal expansion of oil shale is discussed. The following conclusions are drawn:

1. The experiment is carried out to investigate the variation in the specific heat capacity of oil shale samples with temperature. The results show that in the temperature range of 31–390 °C, the growth of the specific heat capacity of oil shale with temperature is regular. However, as the temperature increases from 390 °C to 600 °C, the specific heat capacity of oil shale shows irregular fluctuations due to the pyrolysis of kerogen and the reactions of inorganic minerals such as quartz. It demonstrates that the material composition of oil shale determines its thermophysical properties.
2. According to the thermal expansion experimental results, the thermal expansion rate of oil shale in the vertical bedding direction shows a typical two-stage growth trend. In the first stage, when the oil shale sample is heated from 31 °C to 115 °C, the expansion rate soars, and oil shale is stretched in the vertical bedding direction, facilitating the production of secondary structural surfaces and interlayer fractures and providing preconditions for oil and gas transportation. After the temperature exceeds 115 °C, the increase speed of the expansion rate slows down, but the interlayer fractures continue to propagate and increase, which is conducive to the transportation of oil and gas.
3. In the parallel bedding direction, the thermal expansion of oil shale shows an overall increasing trend and fluctuates in the temperature range of 390–540 °C. Before the temperature reaches 540 °C, K_H decreases precipitously on account of further pyrolysis of kerogen in oil shale, which promotes the generation of new pores and causes damage to its mineral skeleton. After the temperature rises above 540 °C, the thermal expansion rate of oil shale continues to grow, but its growth rate decreases tremendously under the combined influence of inorganic mineral reactions, the continuous growth of thermal stress and the stabilized mineral skeleton.

Acknowledgments

This work was supported by Heilongjiang Provincial Natural Science Foundation of China (No. LH2021E108), the Basic Scientific Research Operating Expenses of Heilongjiang Provincial Universities and Colleges of China (No. 2020-KYYWF-0691) and the National Natural Science Foundation of China (No. 52174075).

The publication costs of this article were partially covered by the Estonian Academy of Sciences.

REFERENCES

1. World Energy Council. *Full Report World Energy Trilemma Index 2022 Report*. https://www.worldenergy.org/publications/entry/world-energy-trilemma-index-2022
2. Xu, Y., Sun, P., Yao, S., Liu, Z., Tian, X., Li, F., Zhang, J. Progress in exploration, development and utilization of oil shale in China. *Oil Shale*, 2019, **36**(2), 285–304. https://doi.org/10.3176/oil.2019.2.03
3. Dyni, J. R. Geology and resources of some world oil-shale deposits. *Oil Shale*, 2003, **20**(3), 193–252.
4. Maaten, B., Loo, L., Konist, A., Nešumajev, D., Pihu, T., Külaots, I. Decomposition kinetics of American, Chinese and Estonian oil shales kerogen. *Oil Shale*, 2016, **33**(2), 167–183. https://doi.org/10.3176/oil.2016.2.05
5. Soone, J., Doilov, S. Sustainable utilization of oil shale resources and comparison of contemporary technologies used for oil shale processing. *Oil Shale*, 2003, **20**(3S), 311–323. https://doi.org/10.3176/oil.2003.3s.04
6. Bai, F., Sun, Y., Liu, Y., Li, Q., Guo, M. Thermal and kinetic characteristics of pyrolysis and combustion of three oil shales. *Energy Convers. Manag.*, 2015, **97**, 374–381. https://doi.org/10.1016/j.enconman.2015.03.007
7. Symington, W. A., Kaminsky, R. D., Meurer, W. P., Otten, G. A., Thomas, M. M., Yeakel, J. D. ExxonMobil's Electrofrac process for in situ oil shale conversion. 236th ACS National Meeting & Exposition, Philadelphia, PA, August 17–21, 2008, In: *Oil Shale: A Solution to the Liquid Fuel Dilemma* (Ogunsola, O. I., Hartstein, A. M., Ogunsola, O., eds.), ACS Sym. Ser, 2010, **1032**, Philadelphia, PA, 185–216. https://doi.org/10.1021/bk-2010-1032.ch010
8. Beer, G., Zhang, E., Wellington, S., Ryan, R., Vinegar, H. Shell's in situ conversion process – factors affecting the properties of produced shale oil. In: *Proceedings of the 28th Oil Shale Symposium*, Golden, Colorado, USA, 13–15 October 2008, Colorado School of Mines, 68.
9. Jaber, J. O., Probert, S. D. Non-isothermal thermogravimetry and decomposition kinetics of two Jordanian oil shales under different processing conditions. *Fuel Process. Technol.*, 2000, **63**(1), 57–70. https://doi.org/10.1016/S0378-3820(99)00064-8
10. Sun, Y., Bai, F., Liu, B., Liu, Y., Guo, M., Guo, W., Wang, Q., Lü, X., Yang, F., Yang, Y. Characterization of the oil shale products derived via topochemical reaction method. *Fuel*, 2014, **115**, 338–346. https://doi.org/10.1016/j.fuel.2013.07.029
11. Liu, Q., Han, X., Li, Q., Huang, Y., Jiang, X. TG–DSC analysis of pyrolysis process of two Chinese oil shales. *J. Therm. Anal. Calorim.*, 2014, **116**(1), 511–517. https://doi.org/10.1007/s10973-013-3524-2

12. Zhang, H., Liu, J., Kang, Z., Yang, D. Experimental research of the pyrolytic properties and mineral components of Bogda oil shale, China. *Oil Shale*, 2018, **35**(3), 214–229. https://doi.org/10.3176/oil.2018.3.02
13. Yan, J., Jiang, X., Han, X., Liu, J. A TG–FTIR investigation to the catalytic effect of mineral matrix in oil shale on the pyrolysis and combustion of kerogen. *Fuel*, 2013, **104**, 307–317. https://doi.org/10.1016/j.fuel.2012.10.024
14. Liu, Z., Ma, H., Guo, J., Liu, G., Wang, Z., Guo, Y. Pyrolysis characteristics and effect on pore structure of Jimsar oil shale based on TG-FTIR-MS analysis. *Geofluids*, **2022**, Article ID 7857239. https://doi.org/10.1155/2022/7857239
15. Liu, Z., Yang, D., Hu, Y., Zhang, J., Shao, J., Song, S., Kang, Z. Influence of in situ pyrolysis on the evolution of pore structure of oil shale. *Energies*, 2018, **11**(4), 755. https://doi.org/10.3390/en11040755
16. Huang, Y., Fan, C., Han, X., Jiang, X. A TGA-MS investigation of the effect of heating rate and mineral matrix on the pyrolysis of kerogen in oil shale. *Oil Shale*, 2016, **33**(2), 125–141. https://doi.org/10.3176/oil.2016.2.03
17. Wang, S., Liu, J., Jiang, X., Han, X., Tong, J. Effect of heating rate on products yield and characteristics of non-condensable gases and shale oil obtained by retorting Dachengzi oil shale. *Oil Shale*, 2013, **30**(1), 27–47. https://doi.org/10.3176/oil.2013.1.04
18. Tiwari, P., Deo, M. Compositional and kinetic analysis of oil shale pyrolysis using TGA–MS. *Fuel*, 2012, **94**, 333–341. https://doi.org/10.1016/j.fuel.2011.09.018
19. Khalil, A. M. Oil shale pyrolysis and effect of particle size on the composition of shale oil. *Oil Shale*, 2013, **30**(2), 136–146. https://doi.org/10.3176/oil.2013.2.04
20. Jaber, J. O., Amri, A., Ibrahim, K. Experimental investigation of effects of oil shale composition on its calorific value and oil yield. *Int. J. Oil, Gas Technol.*, 2011, **4**(4), 307–321. https://doi.org/10.1504/IJOGCT.2011.043714
21. Begum, M., Yassin, M. R., Dehghanpour, H. Effect of kerogen maturity on organic shale wettability: A Duvernay case study. *Mar. Petrol. Geol.*, 2019, **110**, 483–496. https://doi.org/10.1016/j.marpetgeo.2019.07.012
22. El Sayed, A. M. A. Thermophysical study of sandstone reservoir rocks. *J. Petrol. Sci. Eng.*, 2011, **76**(3–4), 138–147. https://doi.org/10.1016/j.petrol.2011.01.001
23. Guo, Y., Li, X., Huang, L. Changes in thermophysical and thermomechanical properties of thermally treated anisotropic shale after water cooling. *Fuel*, 2022, **327**, 125241. https://doi.org/10.1016/j.fuel.2022.125241
24. Abdulagatov, I. M., Abdulagatova, Z. Z., Kallaev, S. N., Bakmaev, A. G., Omarov, Z. M. Heat capacity and thermal diffusivity of heavy oil saturated rock materials at high temperatures. *J. Therm. Anal. Calorim.*, 2020, **142**(1), 519–534. https://doi.org/10.1007/s10973-020-09765-x
25. Verma, A. K., Jha, M. K., Maheshwar, S., Singh, T. N., Bajpai, R. K. Temperature-dependent thermophysical properties of Ganurgarh shales from Bhander group, India. *Environ. Earth Sci.*, 2016, **75**(4), 300. https://doi.org/10.1007/s12665-015-4992-4
26. Arafin, S. Thermophysical properties of reservoir rocks. *J. Phys. Chem. Solids*, 2019, **129**, 99–110. https://doi.org/10.1016/j.jpcs.2018.12.034

27. Huang, Z., Zeng, W., Wu, Y., Li, S., Gu, Q., Zhao, K. Effects of temperature and acid solution on the physical and tensile mechanical properties of red sandstones. *Environ. Sci. Pollut. Res.*, 2021, **28**, 20608–20623. https://doi.org/10.1007/s11356-020-11866-x
28. Tang, F., Wang, L., Lu, Y., Yang, X. Thermophysical properties of coal measure strata under high temperature. *Environ. Earth Sci.*, 2015, **73**, 6009–6018. https://doi.org/10.1007/s12665-015-4364-0
29. Zhu, X., Gao, Z., Chen, T., Wang, W., Lu, C., Zhang, Q. Study on the thermophysical properties and influencing factors of regional surface shallow rock and soil in China. *Front. Earth Sci.*, 2022, **10**, 864548. https://doi.org/10.3389/feart.2022.864548
30. Shaik, S., Ashok Babu, T. P. Influence of ambient air relative humidity and temperature on thermal properties and unsteady thermal response characteristics of laterite wall houses. *Build. Environ.*, 2016, **99**, 170–183. https://doi.org/10.1016/j.buildenv.2016.01.030
31. Li, B., Wang, J., Bi, M., Gao, W., Shu, C. Experimental study of thermophysical properties of coal gangue at initial stage of spontaneous combustion. *J. Hazard. Mater.*, 2020, **400**, 123251. https://doi.org/10.1016/j.jhazmat.2020.123251
32. Khraisha, Y. H. Thermal conductivity of oil shale particles in a packed bed. *Energy Sources*, 2002, **24**(7), 613–623. https://doi.org/10.1080/00908312.2002.11877436
33. Jha, M. K., Verma, A. K., Maheshwar, S., Chauhan, A. Study of temperature effect on thermal conductivity of Jhiri shale from Upper Vindhyan, India. *Bull. Eng. Geol. Environ.*, 2016, **75**, 1657–1668. https://doi.org/10.1007/s10064-015-0829-3
34. Liu, Z., Sun, Y., Guo, W., Li, Q. Reservoir-scale study of oil shale hydration swelling and thermal expansion after hydraulic fracturing. *J. Petrol. Sci. Eng.*, 2020, **195**, 107619. https://doi.org/10.1016/j.petrol.2020.107619
35. Homand-Etienne, F., Houpert, R. Thermally induced microcracking in granites: characterization and analysis. *Int. J. Rock Mech. Min. Sci. Geomech. Abstr.*, 1989, **26**(2), 125–134. https://doi.org/10.1016/0148-9062(89)90001-6
36. Zhao, J., Kang, Z. Permeability of oil shale under in situ conditions: Fushun oil shale (China) experimental case study. *Nat. Resour. Res.*, 2021, **30**(1), 753–763. https://doi.org/10.1007/s11053-020-09717-0
37. Zhao, J., Yang, D., Kang, Z., Feng, Z. A micro-CT study of changes in the internal structure of Daqing and Yan'an oil shales at high temperatures. *Oil Shale*, 2012, **29**(4), 357–367. https://doi.org/10.3176/oil.2012.4.06
38. He, W., Meng, Q., Lin, T., Wang, R., Liu, X., Ma, S., Li, X., Yang, F., Sun, G. Evolution features of in-situ permeability of low-maturity shale with the increasing temperature, Cretaceous Nenjiang Formation, northern Songliao Basin, NE China. *Petr. Explor. Dev.*, 2022, **49**(3), 516–529. https://doi.org/10.1016/S1876-3804(22)60043-0
39. Ma, Z., Xu, L., Gong, P., Chen, Y., Zhang, L. The thermal expansion characteristics of mudstone. *Therm. Sci.*, 2019, **23**(6), 3731–3737. https://doi.org/10.2298/TSCI180718242M

40. Wu, X., Huang, Z., Zhang, S., Cheng, Z., Li, R., Song, H., Wen, H., Huang, P. Damage analysis of high-temperature rocks subjected to LN_2 thermal shock. *Rock Mech. Rock Eng.*, 2019, **52**, 2585–2603. https://doi.org/10.1007/s00603-018-1711-y
41. Zhou, H., Liu, H., Hu, D., Yang, F., Lu, J., Zhang, F. Anisotropies in mechanical behaviour, thermal expansion and P-wave velocity of sandstone with bedding planes. *Rock Mech. Rock Eng.*, 2016, **49**, 4497–4504. https://doi.org/10.1007/s00603-016-1016-y
42. Li, B., Wong, R. C. K. A mechanistic model for anisotropic thermal strain behavior of soft mudrocks. *Engi. Geol.*, 2017, **228**, 146–157. https://doi.org/10.1016/j.enggeo.2017.08.008
43. Yang, D., Wang, G., Kang, Z., Zhao, J., Lv, Y. Experimental investigation of anisotropic thermal deformation of oil shale under high temperature and triaxial stress based on mineral and micro-fracture characteristics. *Nat. Resour. Res.*, 2020, **29**, 3987–4002. https://doi.org/10.1007/s11053-020-09663-x
44. Feng, Z., Qiao, M., Dong, F., Yang, D., Zhao, P. Thermal expansion of triaxially stressed mudstone at elevated temperatures up to 400°C. *Adv. Mater. Sci. Eng*., **2020**, Article ID 8140739. https://doi.org/10.1155/2020/8140739
45. Yu, H., Jiang, X. Influence of particle diameter on pyrolysis property and kinetic parameter of oil shale. *Journal of Zhongyuan University of Technology*, 2007, **78**(1), 1–4 (in Chinese).
46. Zhou, K., Sun, Y., Li, Q., Guo, W., Lv, S., Han, J. Experimental research about thermogravimetric analysis and thermal physical properties of Nong'an oil shale. *Global Geology*, 2016, **35**(4), 1178–1184 (in Chinese).
47. Schärli, U., Rybach, L. Determination of specific heat capacity on rock fragments. *Geothermics*, 2001, **30**(1), 93–110. https://doi.org/10.1016/S0375-6505(00)00035-3
48. Strydom, C. A., Hudson-Lamb, D. L., Potgieter, J. H., Dagg, E. The thermal dehydration of synthetic gypsum. *Thermochim. Acta*, 1995, **269–270**, 631–638. https://doi.org/10.1016/0040-6031(95)02521-9
49. Jaber, J. O., Probert, S. D. Pyrolysis and gasification kinetics of Jordanian oil-shales. *Appl. Energy*, 1999, **63**(4), 269–286. https://doi.org/10.1016/S0306-2619(99)00033-1
50. Bai, F., Sun, Y., Liu, Y., Guo, M. Evaluation of the porous structure of Huadian oil shale during pyrolysis using multiple approaches. *Fuel*, 2017, **187**, 1–8. https://doi.org/10.1016/j.fuel.2016.09.012
51. Saif, T., Lin, Q., Bijeljic, B., Blunt, M. J. Microstructural imaging and characterization of oil shale before and after pyrolysis. *Fuel*, 2017, **197**, 562–574. https://doi.org/10.1016/j.fuel.2017.02.030
52. Savest, N., Oja, V. Heat capacity of kukersite oil shale: Literature overview. *Oil Shale*, 2013, **30**(2), 184–192. https://doi.org/10.3176/oil.2013.2.08
53. Johnson, S. E., Song, W. J., Cook, A. C., Vel, S. S., Gerbi, C. C. The quartz $\alpha \leftrightarrow \beta$ phase transition: Does it drive damage and reaction in continental crust? *Earth Planet. Sci. Lett.*, 2021, **553**, 116622. https://doi.org/10.1016/j.epsl.2020.116622

54. Zhu, Z., Yang, S., Wang, R., Tian, H., Jiang, G., Dou, B. Effects of high temperature on the linear thermal expansion coefficient of Nanan granite. *Acta Geod. Geophys.*, 2022, **57**, 231–243. https://doi.org/10.1007/s40328-022-00375-7
55. Sun, L., Tuo, J., Zhang, M., Wu, C., Wang, Z., Zheng, Y. Formation and development of the pore structure in Chang 7 member oil-shale from Ordos Basin during organic matter evolution induced by hydrous pyrolysis. *Fuel*, 2015, **158**, 549–557. https://doi.org/10.1016/j.fuel.2015.05.061
56. Schrodt, J. T., Ocampo, A. Variations in the pore structure of oil shales during retorting and combustion. *Fuel*, 1984, **63**(11), 1523–1527. https://doi.org/10.1016/0016-2361(84)90219-9
57. Ribas, L., Dos Reis Neto Neto, J. M., França, A. B., Porto Alegre, H. K. The behavior of Irati oil shale before and after the pyrolysis process. *J. Petrol. Sci. Eng.*, 2017, **152**, 156–164. https://doi.org/10.1016/j.petrol.2017.03.007
58. Yu, Y., Liang, W., Bi, J., Geng, Y., Kang, Z., Zhao, Y. Thermophysical experiment and numerical simulation on thermal cracking of oil shale at high temperature. *Chinese Journal of Rock Mechanics and Engineering*, 2015, **34**(6), 1106–1115 (in Chinese).